Biosensors and Bioelectronics 73 (2015) 7–12

Contents lists available at ScienceDirect

Biosensors and Bioelectronics

journal homepage: www.elsevier.com/locate/bios

Electrochemiluminescent DNA sensing using carbon nitride nanosheets as emitter for loading of hemin labeled single-stranded DNA

Yaqiang Feng, Quanbo Wang, Jianping Lei, Huangxian Ju *

State Key Laboratory of Analytical Chemistry for Life Science, School of Chemistry and Chemical Engineering, Nanjing University, Nanjing 210093, China

ARTICLE INFO

Article history:
Received 19 January 2015
Received in revised form
5 May 2015
Accepted 19 May 2015
Available online 21 May 2015

Keywords:
Electrochemiluminescence
Electrocatalysis
Carbon nitride nanosheet
DNA
Hemin

ABSTRACT

Carbon nitride nanosheets (CNNS) have been reported as a cathodic electrochemiluminescence (ECL) emitter in the presence of dissolved oxygen to produce an endogenous coreactant H_2O_2 on electrode surface. This work uses this emitter to construct an ECL sensing platform for sensitive DNA detection through its adsorption ability toward single-stranded DNA (ssDNA). The adsorption of hemin-labeled ssDNA on CNNS leads to *in situ* consumption of dissolved oxygen via hemin-mediated electrocatalytic reduction, thus decreases the formation of coreactant and quenches the ECL emission of CNNS. The ECL sensing platform is designed using hemin-labeled ssDNA to recognize the target DNA, which results in the departure of hemin-labeled hybridization product from the CNNS modified electrode, thus inhibits the annihilation of coreactant and recovers the ECL emission. Under optimized conditions, the proposed sensing strategy shows a wide detection range over 6 orders of magnitude and wondrously high sensitivity with a detection limit down to 2.0 fM. Moreover, the ECL sensor exhibits good performance with excellent selectivity, high reliability, and acceptable fabrication reproducibility. The sensitive sensing strategy provides a new paradigm for the design of ultrasensitive detection method.

1. Introduction

Two-dimensional (2D) nanomaterials, such as graphene, hexagonal boron nitride, transition metal dichalcogenides and transition metal oxides, have received intense scientific attention due to their high specific surface areas and novel electrical and optical properties (Chhowalla et al., 2013; Dresselhaus, 2013; Geim and Grigorieva, 2013; Huang et al., 2013; Nicolosi et al., 2013; Rao et al., 2013; Wang et al., 2012; Xu et al., 2013). Based on interaction between 2D nanomaterials and biomolecules (Ping et al., 2015; Pumera and Loo, 2014), a series of analytical methods have been developed for the detection of wide analytes from protein to small biomolecules. Typically, graphene oxide (GO) has been utilized as a fluorescence platform for the sensitive detection of DNA based on the different affinity with single-stranded DNA (ssDNA) and double-stranded DNA (dsDNA) (He et al., 2010; Lu et al., 2009). Recently, other 2D nanomaterials such as MoS_2 (Zhu et al., 2013), WS_2 (Xi et al., 2014; Yuan et al., 2014), and TiS_2 and TaS_2 (Zhang et al., 2015) have also been used for DNA sensing due to their unique optical properties. Although the 2D nanosheets are continually being updated, these DNA detection methodologies are almost based on fluorescence quenching through fluorescence resonance energy transfer from (He et al., 2010; Lu et al., 2009) or to (Liu et al., 2010) the nanosheets. New detection strategy is very significant for developing biosensing methodology and widening the application of 2D nanosheets.

Electrochemiluminescence (ECL) features intrinsically low background and high sensitivity owing to its electrodriven nature (Hu and Xu, 2010; Lei and Ju, 2011; Miao, 2008; Richter, 2004; Wei and Wang, 2008, 2011; Zhou et al., 2014). A series of materials including Ru complexes, luminol and quantum dots (QDs) have been used to design ECL sensors (Deng and Ju, 2013; Li et al., 2014). Graphite-like carbon nitride (g-C_3N_4) has recently been proved to be an effective ECL emitter (Cheng et al., 2012, 2013). After it is exfoliated into carbon nitride nanosheets (CNNS), the ECL intensity can be greatly enhanced (Chen et al., 2013; Liu et al., 2014). Thus this 2D layered material has been used as the emitter for the constructed of ECL sensor for sensitive determination of dopamine (Liu et al., 2014), carcinoembryonic antigen (Chen et al., 2014), and bisphenol A (Chen et al., 2015) in the presence of $K_2S_2O_8$ or triethylamine as coreactant. Here, its ECL properties were coupled with both its adsorption ability toward ssDNA and the electrocatalytic ability of hemin toward the reduction of dissolved oxygen to construct an ECL DNA sensor through the annihilation of ECL coreactant.

The consumption or generation of ECL coreactant by enzymatic reaction and electrocatalysis is one of ECL sensing mechanisms

* Corresponding author. Fax: +86 25 83593593.
E-mail address: hxju@nju.edu.cn (H. Ju).

http://dx.doi.org/10.1016/j.bios.2015.05.042
0956-5663/

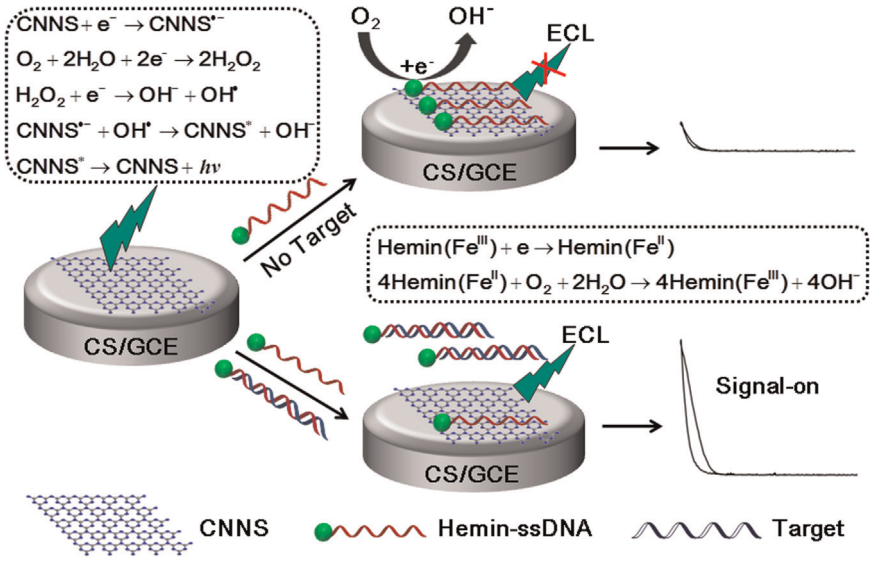

Scheme 1. Schematic illustration of CNNS-based ECL sensing platform for DNA detection.

(Deng and Ju, 2013). Our previous works designed two biosensors by using a hemin/G-quadruplex architecture (Deng et al., 2013a) and hemin-assembled nitrogen-doped graphene (Deng et al., 2013b) to quench the cathodic ECL emission of CdTe QDs through the electrocatalytic reduction of dissolved oxygen. This work designed an electrocatalytic probe, hemin-labeled ssDNA, and adsorbed it on CNNS modified electrode surface to electrocatalyze the reduction of dissolved oxygen, which inhibited the formation of H_2O_2, the coreactant for ECL emission of CNNS (Scheme 1). By hybridization of the hemin-labeled ssDNA with target DNA, the adsorption property was greatly weakened, thus the ECL emission of CNNS modified electrode was recovered, which led to an ECL sensing method for specific detection of DNA. The designed sensing strategy showed a wide detection range over 6 orders of magnitude and a wondrously high sensitivity down to femtomolar level. The excellent analytical performance indicated promising application of 2D nanosheets in ECL bioanalysis.

2. Experimental

2.1. Materials and reagents

Melamine (99%) and chitosan (CS, from crab shell, purity ≥ 85%, deacetylation) were obtained from Sigma-Aldrich Chemical Co., Ltd (Shanghai, China). The chitosan was dispersed in 0.1 M NaAc–HAc buffer (pH 5.0). Potassium persulfate ($K_2S_2O_8$) was purchased from Nanjing Chemical Reagent Co., Ltd (Nanjing, China). The hybridization was performed in Tris–HCl buffer (20 mM, containing 100 mM NaCl, 5.0 mM KCl and 5.0 mM $MgCl_2$, pH 7.4), which was also used as washing buffer. The detection solution was 0.1 M pH 9.0 phosphate buffer saline (PBS), which was prepared by mixing the stock solution of 0.1 M NaH_2PO_4 and 0.1 M Na_2HPO_4 containing 0.1 M KNO_3. All other reagents were analytical grade and used as received. Ultrapure water obtained from a Millipore water purification system (≥ 18 MΩ, Milli-Q, Millipore) was used in all assays.

All synthetic oligonucleotides were purchased from TAKARA Biotechnology (Dalian, China). The probe contained a 5′-hemin label, which was characterized with mass spectrum and high-performance liquid chromatography (Wang et al., 2014). The corresponding sequences are summarized below:

Probe DNA: 5′-hemin-CTGTCTTGAACATGAGTT-3′
Target DNA: 5′-AACTCATGTTCAAGACAG-3′
Single-base mismatched DNA (smDNA): 5′-AACTCATGTTCAA-CACAG-3′
Three-base mismatched DNA (tmDNA): 5′-AACTCATCTTGAA-CACAG-3′

2.2. Apparatus

Atomic force microscopic (AFM) images were acquired on an Agilent 5500 AFM/SPM system (Agilent, USA) in a tapping mode. The samples were prepared by directly casting CNNS dispersion (0.15 mg mL^{-1}) onto freshly cleaved mica sheets. Zeta potential analysis was performed on a Zetasizer (Nano-Z, Malvern, UK). The static water contact angles were measured with a contact angle system (OCA30, Dataphysic Instruments GmbH, Germany) at room temperature using droplets of 8 μL of ultrapure water at the flow of 1 μL s^{-1}. Electrochemical impedance spectroscopic (EIS) measurements were carried out on a PGSTAT30/FRA2 system (Autolab, the Netherlands) in 0.1 M KCl solution containing 5 mM $K_4[Fe(CN)_6]/K_3[Fe(CN)_6]$ (1:1) with frequency from 0.1 Hz to 100 kHz and an amplitude of 5 mV. Cyclic voltammetric (CV) experiments were carried out on a CHI 660B electrochemical workstation (CH Instruments Inc., USA). The ECL measurements were performed in a self-made cell on a MPI-E multifunctional electrochemical and chemiluminescent analytical system (Xi'an Remex Analytical Instrument Co., Ltd. China) with conventional three-electrode configuration. A modified glassy carbon (GCE, 5 mm in diameter) was employed as working electrode with a platinum wire as counter electrode and an Ag/AgCl (saturated KCl) as reference electrode. The ECL emission window was placed in front of the photomultiplier tube (PMT, detection range: 300–650 nm) biased at −1000 V. Unless specially stated, the scan rate was 0.1 V s^{-1}. The ECL experiments were conducted at 25 °C in air-saturated pH 9.0 PBS.

2.3. Preparation of CNNS

The preparation of CNNS was referenced the previous report (Wang et al., 2013). In brief, bulk graphitic-phase carbon nitride (g-C_3N_4) was first synthesized by polymerization of melamin. The CNNS was exfoliated by sonicating bulk g-C_3N_4 in water. The

concentration of as-prepared CNNS was estimated to be 0.15 mg mL^{-1}. Prior to use, the obtained suspension was further concentrated by centrifuging at 12000 rmp for 5 min.

2.4. Preparation of CNNS modified electrode

Prior to modification, a GCE was polished to a mirror using 0.05 μm alumina slurry (Gaoss Union, Wuhan), followed by sonication in water, ethanol and water, respectively. Finally, the electrode was rinsed thoroughly with ultrapure water and dried in nitrogen flow. The 3 μL of CS solution (0.025 wt%) was dropped on GCE surface for improving adhesion force between electrode and CNNS. After drying for about 15 min, 20 μL of CNNS suspension was coated on chitosan surface and dried in air at room temperature overnight.

2.5. ECL detection procedure of target DNA

The "post-mixing" strategy was adopted in the following DNA detection (He et al., 2010). Hemin-labeled ssDNA (hemin-ssDNA) was firstly mixed with different concentrations of target and incubated at 37 °C for 30 min in DNA hybridization buffer. Then 20 μL of the mixture was dropped on the CNNS modified electrode surface. After standing for 10 min, the electrode was carefully rinsed with DNA hybridization buffer. Finally, the ECL signal was detected in 0.1 M pH 9.0 PBS containing 0.1 M KNO_3.

3. Results and discussion

3.1. Characterization and adsorption property of CNNS

The prepared CNNS showed a planar structure with a lateral dimension around 150 nm and the average height around 2 nm (Fig. 1A). Due to the relatively high zeta potential of −28.5 mV, the CNNS could be well dispersed in water without precipitation for several weeks. The contact angle change was used to confirm the different adsorption ability of CNNS toward ssDNA and dsDNA. The contact angle of CNNS/ITO film was measured to be 53.4° (Fig. 1B, a). After the CNNS/ITO film was incubated with hemin-ssDNA, the contact angle decreased to 35.7°, which was attributed to the adsorption of hydrophilic nucleic acid molecules on CNNS surface (Fig. 1B, b). However, after the CNNS/ITO film was incubated with the hybridization product of hemin-ssDNA with target DNA (Fig. 1B, c), the contact angle restored to 51.7°, approximately the same as that of the CNNS/ITO interface. These results indicated the CNNS had much stronger affinity to ssDNA than dsDNA.

3.2. Feasibility and stepwise fabrication of biosensor

To test the feasibility of the proposed ECL biosensing strategy, the effect of dissolved oxygen on the cathodic ECL of CNNS in aqueous solution was first investigated (Fig. 2A). Compared with bare GCE (Fig. 2A, curve a), the CNNS modified GCE showed an efficient cathodic ECL emission at the potential more negative −1.3 V in air-saturated 0.1 M pH 9.0 PBS (Fig. 2A, curve b). However, the cathodic emission almost disappeared after the removal of dissolved oxygen from the same solution (Fig. 2A, curve c), indicating the key role of dissolved oxygen in the ECL process of the immobilized CNNS. The cathodic ECL of CNNS mechanism could be described as follows (Chen et al., 2013):

$$CNNS + e^- \rightarrow CNNS^{\bullet -} \quad (1)$$

$$O_2 + 2H_2O + 2e^- \rightarrow 2H_2O_2 \quad (2)$$

$$H_2O_2 + e^- \rightarrow OH^- + OH^{\bullet} \quad (3)$$

$$CNNS^{\bullet -} + OH^{\bullet} \rightarrow CNNS^* + OH^- \quad (4)$$

$$CNNS^* \rightarrow CNNS + h\nu \quad (5)$$

Obviously the electroreduction product H_2O_2 was the endogenous coreactant of ECL emission of CNNS. After incubation with hemin-ssDNA on the CNNS/CS/GCE surface, the ECL intensity of CNNS decreased by 82.9% (Fig. 2A, curve d), while the ECL intensity quenched only 22.8% after the CNNS/CS/GCE surface was incubated with the hybridization product of the hemin-ssDNA with fully complementary target DNA (Fig. 2A, curve e). This was attributed to the weakened affinity of CNNS to dsDNA (Wang et al., 2013). The formed dsDNA would extricate from CNNS, leading to a decreased amount of hemin on CNNS surface. With the increasing concentration of target DNA, the ECL intensity increased gradually. This led to an ECL method for the detection of DNA concentration.

The stepwise assembly process of the proposed DNA assay was further confirmed by EIS. Fig. 2B shows the impedance spectra of modified electrodes formed in different construction steps and its

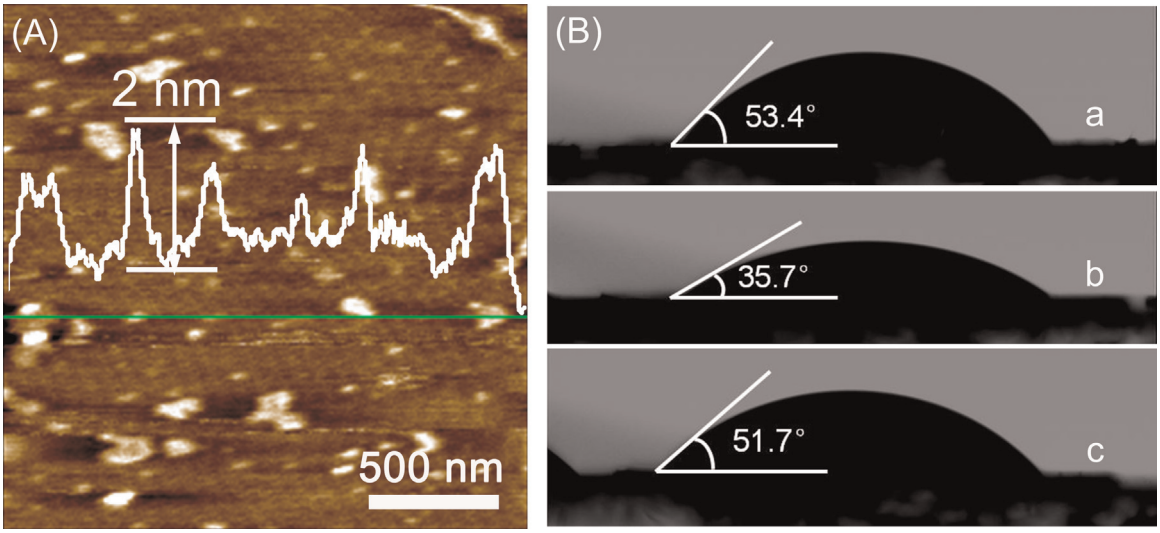

Fig. 1. (A) High-resolution AFM topographic image and corresponding height profile of the as-exfoliated CNNS. (B) Photographic illustration of contact angles of (a) CNNS modified ITO slide, (b) (a) after incubation with hemin-ssDNA, and (c) (a) after incubation with hybridization product of hemin-ssDNA and target DNA.

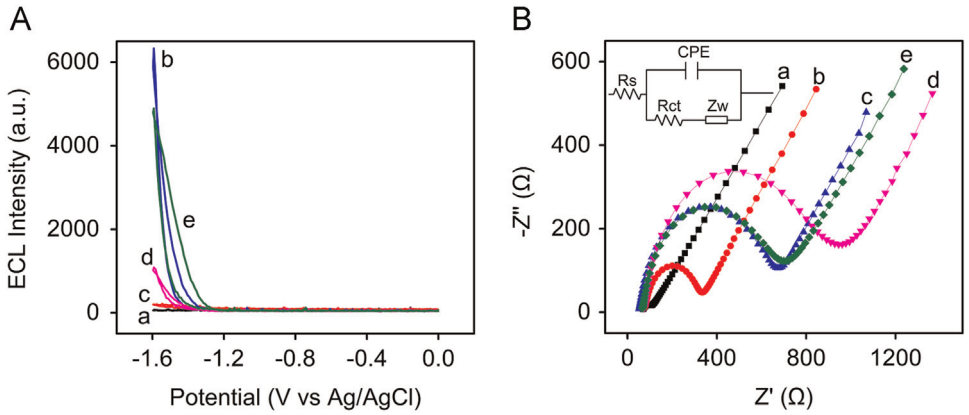

Fig. 2. (A) ECL curves of (a) bare GCE, (b,c) CNNS/CS/GCE in (b) air- and (c) N_2-saturated pH 9.0 PBS, and (d,e) CNNS/CS/GCE after incubation with 20 μL of (d) 1 μM hemin-ssDNA and (e) hybridization product of hemin-ssDNA and target DNA in air-saturated pH 9.0 PBS. (B) EIS plots of (a) bare GCE, (b) CS/GCE, (c) CNNS/CS/GCE, (d) CNNS/CS/GCE after incubation with hemin-ssDNA, and (e) CNNS/CS/GCE after incubation with hybridization product of hemin-ssDNA and target DNA in 0.1 M KCl containing 5 mM $K_4[Fe(CN)_6]/K_3[Fe(CN)_6]$ (1:1). Inset: the electrical equivalent circuit applied to fit the impedance data; R_s, Z_w, R_{ct}, and C_{PE} represent Ohmic resistance of electrolyte, Warburg impedance, charge transfer resistance, and constant phase angle element, respectively.

corresponding equivalent circuit (inset in Fig. 2B). The bare GCE showed a relatively small electron-transfer resistance (R_{ct}) of 90 Ω (Fig. 2B, curve a). After covering with chitosan (Fig. 2B, curve b), the R_{ct} of GCE/CS increased obviously to 281 Ω. When the CNNS was coated on GCE/CS interface (Fig. 2B, curve c), the CNNS/CS/GCE exhibited a higher R_{ct} of 664 Ω due to the intrinsic semiconductivity of CNNS (Cheng et al., 2013). With the assembly of hemin-ssDNA (Fig. 2B, curve d), the value of R_{ct} increased significantly to 972 Ω, which was due to the increase of the steric hindrance from insulating linear aliphatic alkylthiols of ssDNA (Deng et al., 2013a). However, no obvious change (R_{ct} of 686 Ω) was observed when the dsDNA was assembled on the CNNS/CS/GCE (Fig. 2B, curve e), verifying that the CNNS interface had different affinity to dsDNA and ssDNA.

3.3. ECL quenching mechanism

To clarify the quenching mechanism of hemin-ssDNA, persulfate ($K_2S_2O_8$) as cathodic coreactant of ECL emission was added in the detection solution. Upon the cathodic potential scanning at GCE, persulfate was reduced to form strongly oxidizing intermediate ($SO_4^{\bullet-}$). The $SO_4^{\bullet-}$ then oxidized $CNNS^{\bullet-}$ to generate the excited state $CNNS^*$ for emitting light (Chen et al., 2013). In 0.1 M pH 9.0 PBS containing 0.1 M $S_2O_8^{2-}$, the ECL-potential curve of CNNS/CS/GCE showed a strong ECL emission (Fig. 3A, curve a). After incubating the CNNS/CS/GCE with hemin-ssDNA, the ECL decreased by only 12.6 % (Fig. 3A, curve b). The slight decrease could be attributed to the increased R_{ct} (Fig. 2B, curve c to curve d). Thus the corresponding CV showed slight decrease of reduction wave (Inset in Fig. 3A). The negligible CV response of hemin excluded the effect of electron transfer between hemin and electrode on the ECL emission. The ECL decrease was much lower than 82.9% in the absence of $S_2O_8^{2-}$, which indicated the assumption of dissolved oxygen due to its electrocatalytic reduction in the presence of hemin was a main factor in ECL quenching.

In order to further clarify the ECL quenching mechanism of hemin, the CVs of CNNS/CS/GCE after incubation with different concentrations of hemin-ssDNA were examined in the potential window of the oxygen reduction (Fig. 3B). Before incubation with hemin-ssDNA, the CVs of the CNNS/CS/GCE showed one reduction peak at −0.75 V (Fig. 3B, curve a), which was attributed to the electrochemical reduction of dissolved oxygen (Chen et al., 2013). After incubation with different concentrations of hemin-ssDNA, especially at the concentrations more than 100 nM, the reduction peak of dissolved oxygen moved to the around −0.42 V (Fig. 2B, curve c and d). The positively shifted reduction potential indicated an electrocatalytic process of the oxygen reduction by hemin (Deng et al., 2013a). That is, the hemin (Fe^{III}) firstly received one electron from the electrode to form the hemin (Fe^{II}), and then the product was quickly oxidized by dissolved oxygen to transform into OH^- in the alkaline condition, leading to the quenching of the ECL emission. The electrochemical process could be described by the following equations (Deng et al., 2013b):

$$\text{Hemin } (Fe^{III}) + e \rightarrow \text{Hemin } (Fe^{II}) \quad (6)$$

$$4\text{Hemin } (Fe^{II}) + O_2 + 2H_2O \rightarrow 4\text{Hemin } (Fe^{III}) + 4OH^- \quad (7)$$

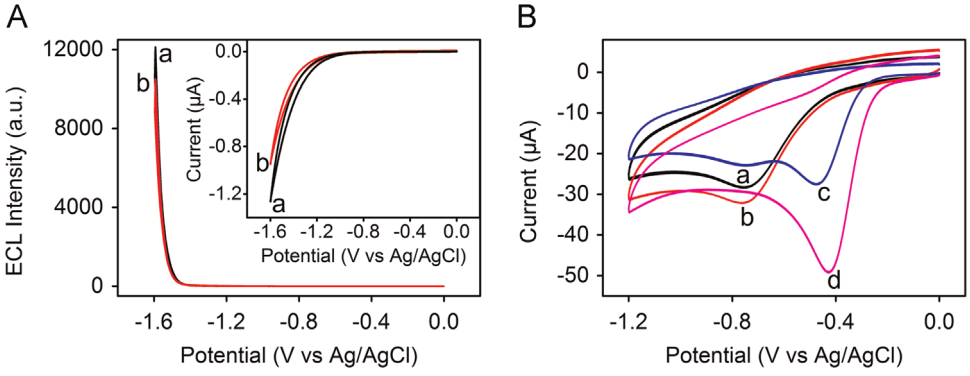

Fig. 3. (A) ECL curves of (a) CNNS/CS/GCE, and (b) CNNS/CS/GCE after incubation with 1 μM hemin-ssDNA in 0.1 M pH 9.0 PBS containing 0.1 M $S_2O_8^{2-}$ as coreactant. Inset: Corresponding CVs. (B) CVs of (a) CNNS/CS/GCE, and (b–d) CNNS/CS/GCE after incubation with 0.1, 1.0 and 10 μM hemin-ssDNA in air -saturated 0.1 M pH 9.0 PBS.

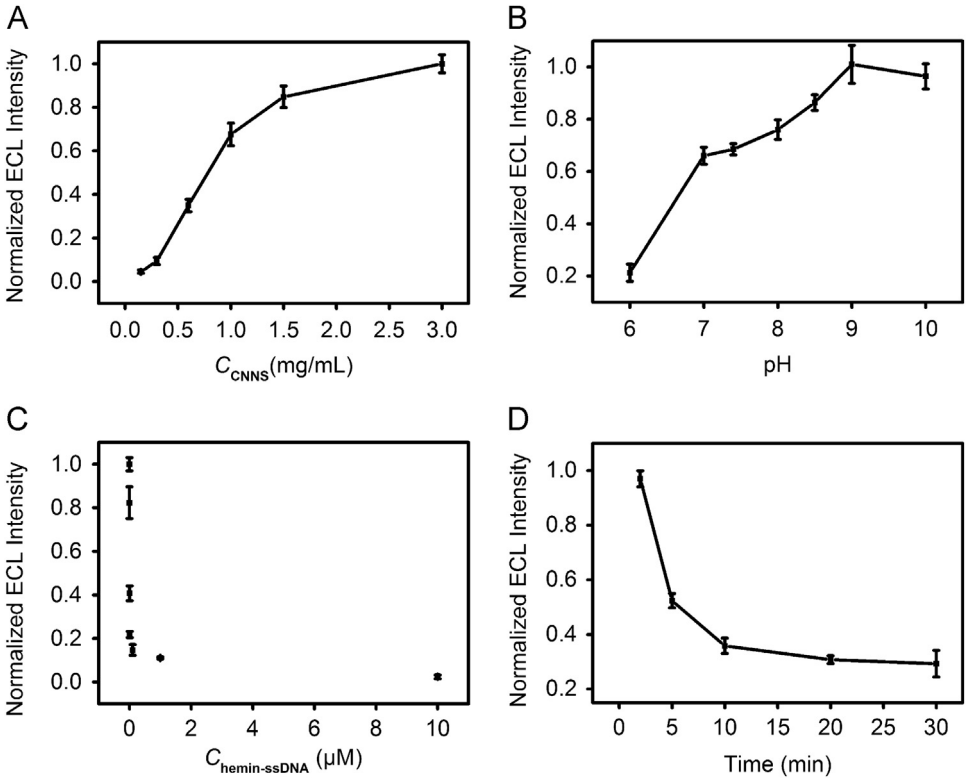

Fig. 4. Dependence of ECL intensity on (A) CNNS concentration for sensor preparation, (B) pH of detection solution, (C) hemin-ssDNA concentration, and (D) adsorption time of hybridization product on CNNS modified electrode at a target concentration of 100 nM. When one parameter changes, the others are at their optimal conditions.

Therefore, it could be concluded that the ECL quenching was due to the electrocatalytic reduction of dissolved oxygen by hemin to consume the dissolved O_2, thus inhibited the formation of the coreactant H_2O_2 for ECL emission of CNNS.

3.4. Optimization of detection conditions

To obtain the good ECL emission of CNNS in PBS, the concentration of CNNS for preparation of modified electrode and the pH of detection solution were optimized. A high concentration of CNNS was favorable for the enhancement of ECL emission and reached the plateau value at 1.5 mg mL^{-1} (Fig. 4A). The effect of pH on the ECL response is shown in Fig. 4B. In the experimental pH range, the ECL intensity increased with the increasing pH value and then reached a maximum at pH 9.0. This result could be attributed to the fact that the electrogenerated intermediates of dissolved oxygen (e.g., $OH^{\bullet}$) were more stable at high pH, which was favorable for the enhancement of the ECL emission. Thus, 1.5 mg mL^{-1} CNNS and pH 9.0 were employed for the following experiments.

As the ECL quenching was controlled by the electrocatalyis of hemin-ssDNA toward the reduction of dissolved oxygen, the ECL emission dropped drastically with the increasing concentration of hemin-ssNDA and then remained steady at 0.1 μM (Fig. 4C), indicating a saturated adsorption of hemin-ssDNA on the CNNS modified electrode. The adsorption time of hybridization product on CNNS modified electrode surface was also examined. As shown in Fig. 4D, the ECL intensity quickly decreased and reached a steady value at about 10 min, indicating the saturated adsorption of the hemin-ssDNA left in hybridization product. Thus, the concentration of hemin-ssDNA was chosen as 0.1 μM and the adsorption time was settled at 10 min.

3.5. ECL detection of target DNA

Under the optimum conditions, the ECL peak intensity gradually increased with the increment of the target DNA concentration (Fig. 5A). The calibration plot showed a linear response between ECL intensity and the logarithmic value of target DNA concentration ranging from 10 fM to 10 nM (Fig. 5B). The regression equation was $I=529.4\times\log C+1263.5$ with a correlation coefficient of 0.992, where I is ECL peak intensity and C is the concentration of target DNA (pM). The detection limit calculated from three times standard deviation of the blank measurements and the slope was 2.0 fM, which was lower than that using ruthenium complex functionalized graphene oxide as ECL-DNA sensing platform (Li et al., 2014). More importantly, the developed DNA sensor showed a wide detection range of six orders of magnitude, which was wider than those of previously reported homogeneous fluorescence sensing platform based on 2D nanomaterials, such as GO (He et al., 2010), MoS_2 nanosheets (Zhu et al., 2013), WS_2 nanosheets (Yuan et al., 2014), TiS_2 and TaS_2 nanosheets (Zhang et al., 2015).

The proposed method also showed good specificity for sequence detection of the target DNA. As shown in Fig. 5C, fully complementary target DNA, smDNA and tmDNA showed the ECL response of 6.58, 1.93, and 1.57 times that to blank (hemin-ssDNA/CNNS/CS/GCE), respectively. In addition, both the intra-assay and inter-assay precisions of the proposed method were examined at 1.0 nM target DNA. The five measurements showed the relative standard deviations (RSD) of 3.8% and 8.7%, respectively, indicating good precision and acceptable fabrication reproducibility. Five measurements of the ECL emission upon continuous cyclic scans of the proposed biosensor showed a coincident signal with RSD of 5.2% (Fig. 5D), indicating acceptable reliability and stability of the detection signal. These results revealed that the proposed ECL biosensor has a good performance for DNA detection.

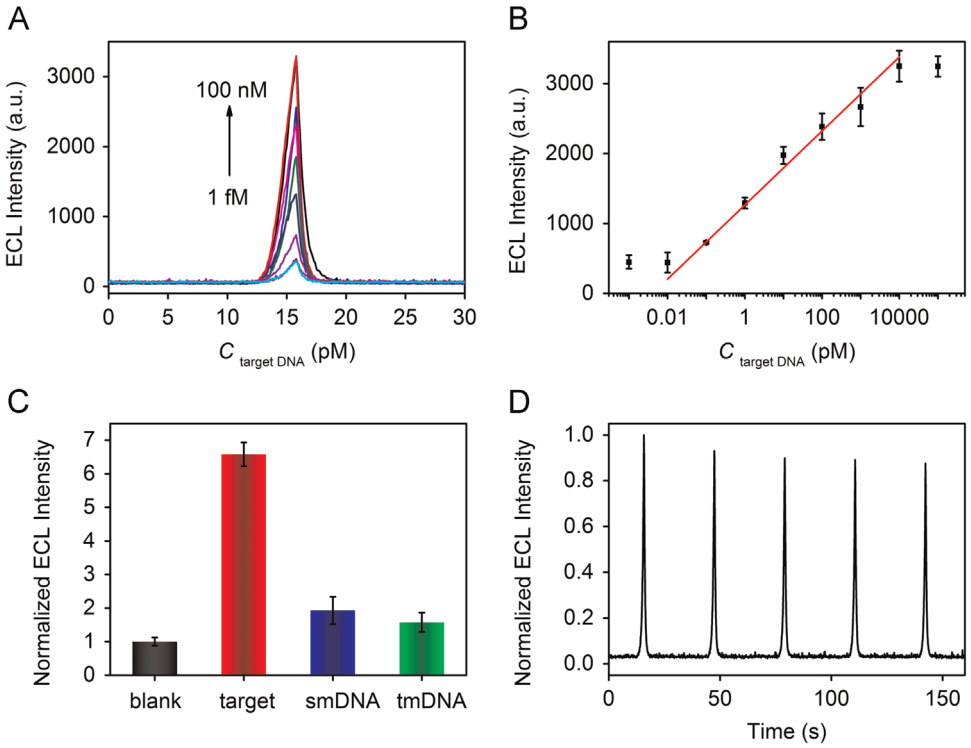

Fig. 5. (A) ECL responses of the proposed sensor to target DNA at 1 fM, 10 fM, 100 fM, 1 pM, 10 pM, 100 pM, 0.1 nM, 10 nM, and 100 nM. (B) Calibration curve ($n=3$). (C) Relative ECL responses to blank, 1.0 nM target DNA, 1.0 nM smDNA and 1.0 nM tmDNA in presence of 100 nM hemin-ssDNA, respectively. (D) Continuous cyclic scans of the ECL sensor in air-saturated 0.1 M pH 9.0 PBS.

4. Conclusion

This work demonstrates that the two-dimension CNNS as an ECL emitter can be successfully applied in the detection of DNA. The CNNS not only provides ECL signal, but also can distinguish ssDNA and dsDNA with a hemin-labeled ssDNA as probe to recognize the target DNA. The adsorption of hemin-labeled ssDNA on CNNS quenches the ECL emission through the electrocatalytic reduction of dissolved oxygen by the adsorbed hemin, which inhibits the formation of H_2O_2 as an endogenous coreactant. The proposed ECL biosensor for DNA is simple and efficient. It exhibits high sensitivity with detection limit down to femtomolar level and a wide linear range over 6 orders of magnitude. This work provides a new paradigm for the detection of DNA using two-dimensional emitter and expands the application of these materials in ECL biosensing and clinical diagnosis.

Acknowledgments

This work was financially supported by National Natural Science Foundation of China (21121091, 21135002, 91413118) and Priority development areas of the National Research Foundation for the Doctoral Program of Higher Education of China (20130091130005).

References

Chen, L.C., Huang, D.J., Ren, S.Y., Dong, T.Q., Chi, Y.W., Chen, G.N., 2013. Nanoscale 5, 225–230.
Chen, L.C., Zeng, X.T., Ferhan, A.R., Chi, Y.W., Kim, D.H., Chen, G.N., 2015. Chem. Commun. 51, 1035–1038.
Chen, L.C., Zeng, X.T., Si, P., Chen, Y.M., Chi, Y.W., Kim, D.H., Chen, G.N., 2014. Anal. Chem. 86, 4188–4195.
Cheng, C.M., Huang, Y., Tian, X.Q., Zheng, B.Z., Li, Y., Yuan, H.Y., Xiao, D., Xie, S.P., Choi, M.M.F., 2012. Anal. Chem. 84, 4754–4759.
Cheng, C.M., Huang, Y., Wang, J., Zheng, B.Z., Yuan, H.Y., Xiao, D., 2013. Anal. Chem. 85, 2601–2605.
Chhowalla, M., Shin, H.S., Eda, G., Li, L.-J., Loh, K.P., Zhang, H., 2013. Nat. Chem. 5, 263–275.
Deng, S.Y., Cheng, L.X., Lei, J.P., Cheng, Y., Huang, Y., Ju, H.X., 2013a. Nanoscale 5, 5435–5441.
Deng, S.Y., Ju, H.X., 2013. Analyst 138, 43–61.
Deng, S.Y., Lei, J.P., Huang, Y., Cheng, Y., Ju, H.X., 2013b. Anal. Chem. 85, 5390–5396.
Dresselhaus, M.S., 2013. Mater. Res. Lett., 1–9.
Geim, A.K., Grigorieva, I.V., 2013. Nature 499, 419–425.
He, S.J., Song, B., Li, D., Zhu, C.F., Qi, W.P., Wen, Y.Q., Wang, L.H., Song, S.P., Fang, H.P., Fan, C.H., 2010. Adv. Funct. Mater. 20, 453–459.
Hu, L.Z., Xu, G.B., 2010. Chem. Soc. Rev. 39, 3275–3304.
Huang, X., Zeng, Z.Y., Zhang, H., 2013. Chem. Soc. Rev. 42, 1934–1946.
Lei, J.P., Ju, H.X., 2011. TrAC Trends Anal. Chem. 30, 1351–1359.
Li, F., Yu, Y.Q., Li, Q., Zhou, M., Cui, H., 2014. Anal. Chem. 86, 1608–1613.
Liu, F., Choi, J.Y., Seo, T.S., 2010. Biosens. Bioelectron. 25, 2361–2365.
Liu, Y.T., Wang, Q.B., Lei, J.P., Hao, Q., Wang, W., Ju, H.X., 2014. Talanta 122, 130–134.
Lu, C.H., Yang, H.H., Zhu, C.L., Chen, X., Chen, G.N., 2009. Angew. Chem. Int. Ed. 48, 4785–4787.
Miao, W.J., 2008. Chem. Rev. 108, 2506–2553.
Nicolosi, V., Chhowalla, M., Kanatzidis, M.G., Strano, M.S., Coleman, J.N., 2013. Science 340, 1226419.
Ping, J.F., Zhou, Y.B., Wu, Y.Y., Papper, V., Boujday, S., Marks, R.S., Steele, T.W.J., 2015. Biosens. Bioelectron. 64, 373–385.
Pumera, M., Loo, A.H., 2014. TrAC Trends Anal. Chem. 61, 49–53.
Rao, C.N.R., Ramakrishna Matte, H.S.S., Maitra, U., 2013. Angew. Chem. Int. Ed. 52, 13162–13185.
Richter, M.M., 2004. Chem. Rev. 104, 3003–3036.
Wang, Q.B., Wang, W., Lei, J.P., Xu, N., Gao, F.L., Ju, H.X., 2013. Anal. Chem. 85, 12182–12188.
Wang, Q.B., Xu, N., Lei, J.P., Ju, H.X., 2014. Chem. Commun. 50, 6714–6717.
Wang, Q.H., Kalantar-Zadeh, K., Kis, A., Coleman, J.N., Strano, M.S., 2012. Nat. Nanotechnol. 7, 699–712.
Wei, H., Wang, E.K., 2008. TrAC Trends Anal. Chem. 27, 447–459.
Wei, H., Wang, E.K., 2011. Luminescence 26, 77–85.
Xi, Q., Zhou, D.M., Kan, Y.Y., Ge, J., Wu, Z.K., Yu, R.Q., Jiang, J.H., 2014. Anal. Chem. 86, 1361–1365.
Xu, M.S., Liang, T., Shi, M.M., Chen, H.Z., 2013. Chem. Rev. 113, 3766–3798.
Yuan, Y.X., Li, R.Q., Liu, Z.H., 2014. Anal. Chem. 86, 3610–3615.
Zhang, Y., Zheng, B., Zhu, C.F., Zhang, X., Tan, C.L., Li, H., Chen, B., Yang, J., Chen, J.Z., Huang, Y., Wang, L.H., Zhang, H., 2015. Adv. Mater. 27, 935–939.
Zhou, X.M., Zhu, D.B., Liao, Y.H., Liu, W.P., Liu, H.X., Ma, Z.K., Xing, D., 2014. Nat. Protoc. 9, 1146–1159.
Zhu, C.F., Zeng, Z.Y., Li, H., Li, F., Fan, C.H., Zhang, H., 2013. J. Am. Chem. Soc. 135, 5998–6001.